Virology 426 (2012) 143–151

Contents lists available at SciVerse ScienceDirect

Virology

journal homepage: www.elsevier.com/locate/yviro

Crystal structures of murine norovirus-1 RNA-dependent RNA polymerase in complex with 2-thiouridine or ribavirin

Intekhab Alam [a], Ji-Hye Lee [a], Ki Joon Cho [a], Kang Rok Han [b], Jai Myung Yang [b], Mi Sook Chung [c,*], Kyung Hyun Kim [a,**]

[a] Department of Biotechnology & Bioinformatics, Korea University, Chungnam 339-700, Republic of Korea
[b] Department of Life Science, Sogang University, Seoul 121-742, Republic of Korea
[c] Department of Food and Nutrition, Duksung Women's University, Seoul 132-714, Republic of Korea

ARTICLE INFO

Article history:
Received 20 October 2011
Returned to author for revision
16 November 2011
Accepted 18 January 2012
Available online 16 February 2012

Keywords:
Norovirus
RNA-dependent RNA polymerase
Crystal structure
2-thiouridine
Ribavirin
Viral inhibition

ABSTRACT

Murine norovirus-1 (MNV-1) shares many features with human norovirus (HuNoV) and both are classified within the norovirus genus of *Caliciviridae* family. MNV-1 is used as the surrogate for HuNoV research since it is the only form that can be grown in cell culture. HuNoV and MNV-1 RNA dependent RNA polymerase (RdRp) proteins with the sequence identity of 59% show essentially identical conformations. Here we report the first structural evidence of 2-thiouridine (2TU) or ribavirin binding to MNV-1 RdRp, based on the crystal structures determined at 2.2 Å and 2.5 Å resolutions, respectively. Cellular and biochemical studies revealed stronger inhibitory effect of 2TU on the replication of MNV-1 in RAW 264.7 cells, compared to that of ribavirin. Our complex structures highlight the key interactions involved in recognition of the nucleoside analogs which block the active site of the viral RNA polymerase.

Introduction

The genus norovirus (NV) in the *Caliciviridae* family causes approximately 90% of epidemic non-bacterial outbreaks of gastroenteritis around the world (Green, 2007; Lindesmith et al., 2003), commonly referred to as the gastric flu. Due to the lack of an efficient cell-culture system and an animal model to study virus propagation, human NV (HuNoV) has been relatively understudied. Murine norovirus-1 (MNV-1) from STAT1-deficient (STAT1−/−) mice was successfully grown in the macrophage cell line RAW 264.7 (Wobus et al., 2004, 2006) and has served as a surrogate model system for studying norovirus biology and pathogenesis. However, the molecular mechanisms of NV replication and pathogenesis remain poorly understood.

The NV genome of a positive-sense single-stranded RNA encodes three open reading frames: ORF-2 encodes the capsid protein (VP1), ORF-3 encodes the virion protein 2 (VP2), and ORF-1 encodes non-structural proteins (Green, 2007; Karst et al., 2003). Studies on NV RNA replication has focused on the *in vitro* functions of non-structural proteins. RNA-dependent RNA polymerase (RdRp) which is involved in synthesis and amplification of viral genome uses ribonucleotide triphosphate (rNTPs) as substrate with low fidelity and lacks an error-prone repair mechanism. This virally encoded RdRp is one of the key targets for the development of novel antiviral agents (Zamyatkin et al., 2008). Nucleoside analogs such as ribavirin and 5-fluorouracil were shown to induce error in the viral replication (Ferrer-Orta et al., 2007). The biochemical evidence for the inhibition of NV replication by ribavirin and IFN-γ in replicon-bearing cells was previously reported (Chang and George, 2007). Detailed studies on the mechanism of inhibition have shown that ribavirin is incorporated into viral RNA where it base pairs with UMP or CMP and drives different RNA viruses towards extinction through enhanced mutagenesis (Crotty et al., 2000; Lau et al., 2002). Ribavirin is used as an antiviral prodrug which is metabolized to active 5′-monophosphate, diphosphate and triphosphate *in vivo* (Wu et al., 2003). Biochemical studies with 2-thiouridine (2TU) revealed that it not only inhibits the norovirus polymerase but also has inhibitory effect on viral growth of CRFK cells in feline calicivirus (FCV) (Belliot et al., 2005).

A high resolution crystal structure is required to rationalize the inhibitory activity of these compounds on viral RdRp. The only structure available for the viral polymerase in complex with ribavirin is that of foot and mouth disease virus (FMDV) which showed the binding of ribavirin at the active site (Ferrer-Orta et al., 2007), while structural evidence for binding of 2TU with viral RdRp is lacking. The structures

* Correspondence to: M.-S. Chung, Department of Food and Nutrition, Duksung Women's University, Seoul 132-714, Republic of Korea. Fax: +82 2 901 8372.
** Correspondence to: K.H. Kim, Department of Biotechnology & Bioinformatics, Korea University, Chungnam 337-800, Republic of Korea. Fax: +82 2 3290 3945.
E-mail addresses: mschung@duksung.ac.kr (M.S. Chung), khkim@korea.ac.kr (K.H. Kim).

0042-6822/$ – see front matter © 2012 Elsevier Inc. All rights reserved.
doi:10.1016/j.virol.2012.01.016

of NV RdRp in complex with template RNA duplex and nucleotides were reported (Zamyatkin et al., 2008, 2009). These structures provide valuable insight about the mechanism involved in recognition and positioning of nucleotides at the active site of RdRp.

In the present study we have solved the structures of MNV-1 RdRp in complex with 2TU or ribavirin and have studied their inhibitory effects on MNV-1 replication in RAW 264.7 cells. To our knowledge this is the first structural report describing the binding modes of 2TU and ribavirin in calicivirus RdRp and the first inhibitory report of 2TU on MNV-1 in RAW 264.7 cells. In the light of novel therapeutic strategies aiming at blocking the replication complex of NV through inhibition of viral enzyme interaction, our results can be used to design some rational antiviral compounds for noroviral RNA polymerases.

Results and discussion

Effect of 2TU or ribavirin on MNV-1 in infected cells and RdRp enzyme

Two commercially available viral nucleoside analogs (2TU and ribavirin) were tested for their inhibitory effect on the growth of MNV-1 in RAW 264.7 cells. Although the inhibitory activity of ribavirin has been studied previously (Chang and George, 2007), the activity of 2TU on the growth of MNV-1 has not been documented. Within the non-cytotoxic range of concentrations (0–100 μM), both 2TU and ribavirin were found to exhibit an inhibitory effect on the replication of MNV-1 in RAW 264.7 cells (Fig. 1A). A concentration of ~25 μM of 2TU was sufficient to reach 50% of inhibition of MNV-1 induced cell death. Notably, the inhibitory effect of 2TU was significantly higher (up to 5-fold) than that of ribavirin. This observation was in accordance with the previously published report for the inhibition of FCV replication in CRFK cells (Belliot et al., 2005), where 2TU was found to be more potent than ribavirin. Both plaque reduction and RT-PCR analysis further proved the potency of 2TU where 10 μM of 2TU was sufficient to significantly reduce the level of viral plaque formation and RdRp gene expression, respectively (Figs. 1B and C). Simultaneous and post-treatment of 2TU or ribavirin produced higher inhibitory effect on cell death than pre-treatment.

To study the possible interactions between MNV-1 RdRp and ligands, the effects of temperature on protein stability were monitored by differential scanning fluorimetry (DSF), in which the extent of the temperature shift in denaturation profiles is proportional to the affinity of the ligand for a given protein (Vedadi et al., 2006). A ligand concentration of 10–20 mM was necessary to shift the T_m by 2–3 °C. The transition temperature (T_m) of RdRp native was 36.5 °C, whereas it was 38.5 °C and 39.5 °C for the ribavirin and 2TU complexes, respectively (Fig. 1D). This result complemented the viral inhibition studies described above, suggesting the binding of 2TU or ribavirin

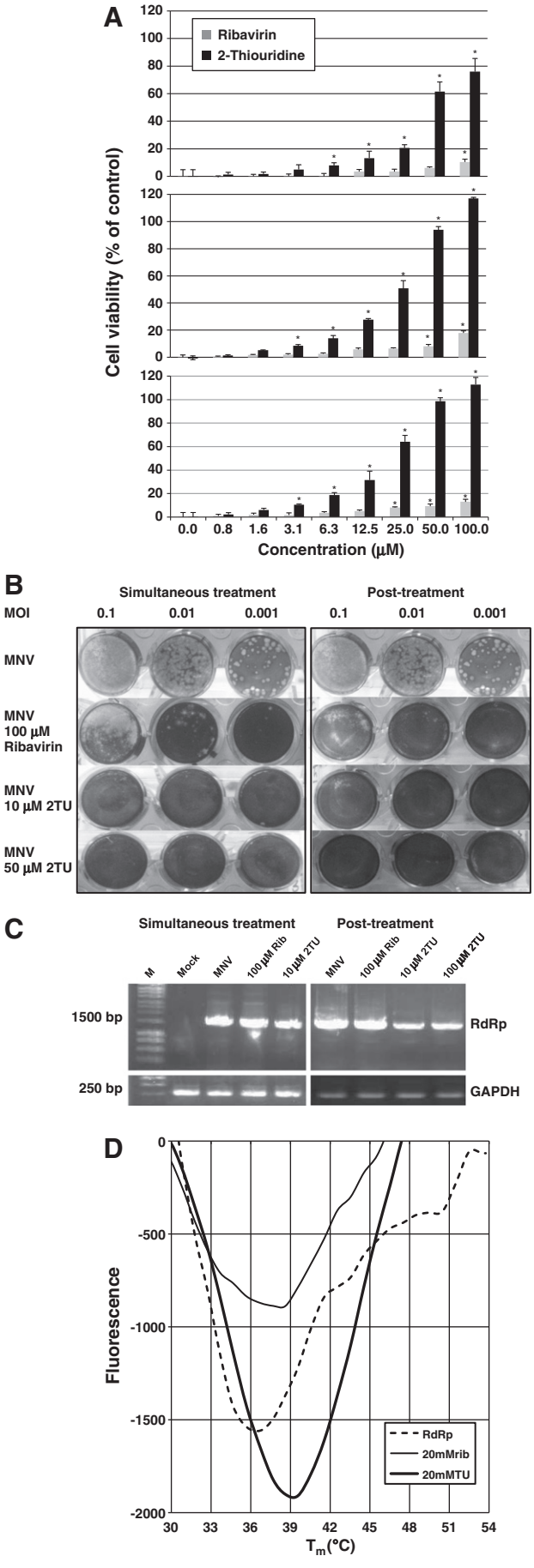

Fig. 1. Viral inhibition and DSF analysis. (A) Effects of 2TU (black) or ribavirin (light gray) on MNV-1 infection in RAW 264.7 cells. Pre-treatment of RAW 264.7 cells with 2TU or ribavirin in various concentrations for 1 hr followed by infection with MNV-1 at MOI of 0.01 using 96-well plates (upper panel), Simultaneous-treatment with MNV-1 in the presence of 2TU or ribavirin (middle panel), and post-treatment with MNV-1 for 1 hr followed by the addition of 2TU or ribavirin in various concentrations (lower panel). The virus infected cells were incubated for an additional 3 days and MNV-1 induced cytopathic effect (CPE) was determined by MTT cell viability reduction assay. Error bars represent standard deviations from at least three replicates. Values obtained from non-infected and infected cells by MNV-1 only in the absence of ribavirin or 2TU were 2.169 ± 0.09 and 0.266 ± 0.05, respectively, showing MNV-1 induced CPE. Significant increase in cell viability was indicated by asterisks ($P<0.05$) and mean ± standard deviations were shown from at least three replicates. (B) Plaque reduction assay. MNV plaques were compared at different MOI at simultaneously treated in MNV innoculum (left panel) or treated post-infection on the cells (right panel). (C) Effects of 2TU or ribavirin on MNV infection to the cells analyzed by RT-PCR. Simultaneous treatment during MNV inoculation (left panel) and post-treatment (right panel) at concentrations of 10–100 μM. Cells were harvested and viral RNA RdRp gene was analyzed by RT-PCR with GAPDH as endogenous control gene. (D) Differential scanning Fluorimetry (DSF) transition curves of MNV-1 RdRp in the presence of 2TU or ribavirin.

with MNV-1 RdRp. Within the same concentration range of ligands, T_m value shift was higher for 2TU (~3 °C) in comparison to ribavirin (~2 °C), suggesting the higher affinity of 2TU than ribavirin. Similar studies have been performed in poliovirus polymerase where addition of NTP increases the T_m value by 5–6 °C (Thompson et al., 2007). To determine the strength of binding for these ligands (2TU and ribavirin) isothermal titration calorimetry experiments were carried out to determine the affinity (K_d) of ligands with the protein. MNV-1 RdRp binds to 2TU with a $K_d = 0.865 \pm 0.4$ μM, although we failed to get a K_d for ribavirin despite trying various concentrations of ligand and protein. Based on the results of cytopathic effect, plaque reduction assay, RT-PCR, and DSF, ribavirin is likely to have much lower value of K_d to MNV-1 RdRp, in comparison to 2TU. In fact, there are no reports available for the K_d of viral RdRp with ribavirin.

Overall structures

The overall structures of MNV-1 RdRp in complex with the ligand (2TU or ribavirin) revealed a right hand fold with palm, fingers, thumb, and N-terminal domains (Supplementary Fig. S1), which was essentially identical to those reported previously (Ferrer-Orta et al., 2007; Hogbom et al., 2009; Lee et al., 2011; Ng et al., 2004; Zamyatkin et al., 2008; Zamyatkin et al., 2009). It adopts an enclosed conformation where the extended N-terminal domain bridges across the fingers and thumb domains. Structural superposition using secondary structure matching (SSM) (Krissinel and Henrick, 2004) between the native (PDB ID: 3QID) and 2TU or ribavirin-complexed structures of MNV-1 RdRp gave an r.m.s.d of 0.46 Å or 0.64 Å, respectively. The ligand complexed structures (2TU and ribavirin) showed a few variations from that of native in the loop regions comprising of residues 374–381, 434–440 and 466–478 (data not shown). The loop region comprising of these residues are not superposed well with that of native structure. These structural differences are attributed to the intrinsic flexibility of the loops which were also reported in other viral polymerase structures (Hogbom et al., 2009; Ng et al., 2004). In the 2TU-complex structure, residues 468–475 in chain A and residues 437–440 and 467–474 in chain B were missing due to lack of convincing electron density, and residues 467–474 in chains A and C were not modeled in the ribavirin complex. In contrast, the same loops were well resolved in all the three chains of the native and 5-fluorouracil (5FU)-complex structures of MNV-1 RdRp (Lee et al., 2011). The amino acid residues in these loops of the 2TU or ribavirin complex structure showed the highest B factors, indicating increased flexibility in the crystal. The complex structures suggest that the presence of ligand might have disrupted local crystal packing, possibly resulting in the perturbation of loops of the monomers in the asymmetric unit. The loop regions were also reported to be perturbed in HuNoV RdRp in complex with CTP and NCT (Zamyatkin et al., 2008).

Interestingly, disulfide bond formation was observed between Cys206 and Cys307 in the 2TU or ribavirin complex structure of MNV-1 RdRp, which was not observed in the native as well as the 5FU-complex of MNV-1 RdRp (Supplementary Fig. S2). It was also observed in an archaeal RNA polymerase but its biological significance has not been described (Hirata et al., 2008). The amino acid residue Cys307 which is close to the active site was found to move toward Cys206 forming a disulfide bond. Given that the crystallization conditions for both the ligand complexes as well as the native enzyme were almost identical, it is highly likely that the ligand binding induces a conformational change which is stabilized by disulfide bond formation between Cys206 and Cys307.

The MNV-1 RdRp–ligand complexes

Initial attempt to get the crystal structure of the MNV-1 RdRp–ligand complex by soaking the enzyme crystals with ligands in different soaking time and concentrations was not successful and soaking with 2TU seriously cracked the crystals. The ligands were dissolved in DMSO which seems to have a damaging effect on RdRp crystal packing. As soaking with ligands was not successful, we switched over to co-crystallization of the complex. The crystal structure of FMDV RdRp in complex with ribavirin triphosphate (RTP) was obtained by soaking RdRp with RTP for 6 hrs (Ferrer-Orta et al., 2007). Initial analysis of the difference electron density maps between the complex and the native showed the presence of extra density that would correspond to the ligand occupying a position at the active site of MNV-1 RdRp (Supplementary Fig. S3). The resulting $2F_o–F_c$ and $F_o–F_c$ electron density and composite omit maps substantiated the location and orientation of 2TU or ribavirin and careful manual rebuilding with further refinement allowed confident assignment of surrounding amino acid residues that were omitted from the initial model to eliminate model bias (Figs. 2A and B). There are three molecules in the asymmetric unit and the map feature was found to be better in chains A and C of the 2TU complex as compared to chains A and B of the ribavirin complex. Modeling was done in all the three chains of 2TU or ribavirin with different occupancies: 2TU with occupancy of 0.69 in chain A and 0.57 in chains B and C, and ribavirin with occupancy of 0.78 in A and B and 0.80 in chain C. The average B factors for 2TU were 38.3 $Å^2$, 42.5 $Å^2$ and 35.4 $Å^2$ and those for ribavirin were 38.5 $Å^2$, 55 $Å^2$ and 70.8 $Å^2$ for chains A, B and C, respectively. The presence of significant electron density together with relatively high occupancy of the ligands indicates relatively tight binding for 2TU in comparison to ribavirin as evident from the dissociation constant ($K_d = 0.865 \pm 0.4$ μM), DSF and RT-PCR studies carried out in the presence of the ligand.

The structural superposition of three individual RdRp monomers in the 2TU and ribavirin complexes showed r.m.s.d values of 0.6–0.8 Å and 0.4–0.6 Å, respectively. The binding orientation of 2TU in monomer A was slightly different from that in monomer B (Supplementary Fig. S4). The ambiguity in chain B could be attributed to the weak electron density map as well as the resolution limits of the dataset, at which it was difficult to ascertain the correct orientation of the molecule. Similarly in the ribavirin complex structure, the ligand molecule showed slightly different orientation in different chains (Supplementary Fig. S4), but the binding mode was similar. This difference can be attributed to the local conformational changes in the side chains of amino acids at the active site.

Superimposing the structures of the 2TU and ribavirin complexes using SSM gave r.m.s.d of 0.5 Å, indicating relatively low variability in the ligand-bound structures of MNV-1 RdRp. However, a comparison of the active site between the native and the complexes revealed interesting structural features. First, the amino acid residues involved in the interaction with metal ions and 2TU or ribavirin were well superimposed except for two arginine residues Arg185 and Arg395 (Fig. 3A). Deviation was significantly higher in Arg395 than Arg185. The B-factors for the side chains in the native structure were in the range of 40–45 $Å^2$, whereas those in the 2TU complex were 70 $Å^2$ for Arg395 and 45 $Å^2$ for Arg185. In the ribavirin complex, the B factors for Arg185 and Arg395 were 50 and 80 $Å^2$, respectively. Higher B-factors of the residue in the complex structures suggest local conformational changes upon ligand binding.

Second, superposition of the RdRp structures in complex with the ligand (2TU or ribavirin) and 5FU of which the complex structure was previously reported (Lee et al., 2011) showed an r.m.s.d of 0.7 Å. The active site is rich in aspartate residues which are highly conserved and actively involved in RdRp enzyme catalysis. These residues underwent conformational changes that were different from those induced by 5FU binding. Residues Asp243 and Asp245 were oriented differently at the active site of both the 2TU- and ribavirin-bound complexes in comparison to that found in the 5FU-bound complex structure (data not shown). It was also noticeable that the side chain orientation of Arg395 in the 2TU or ribavirin complex structure

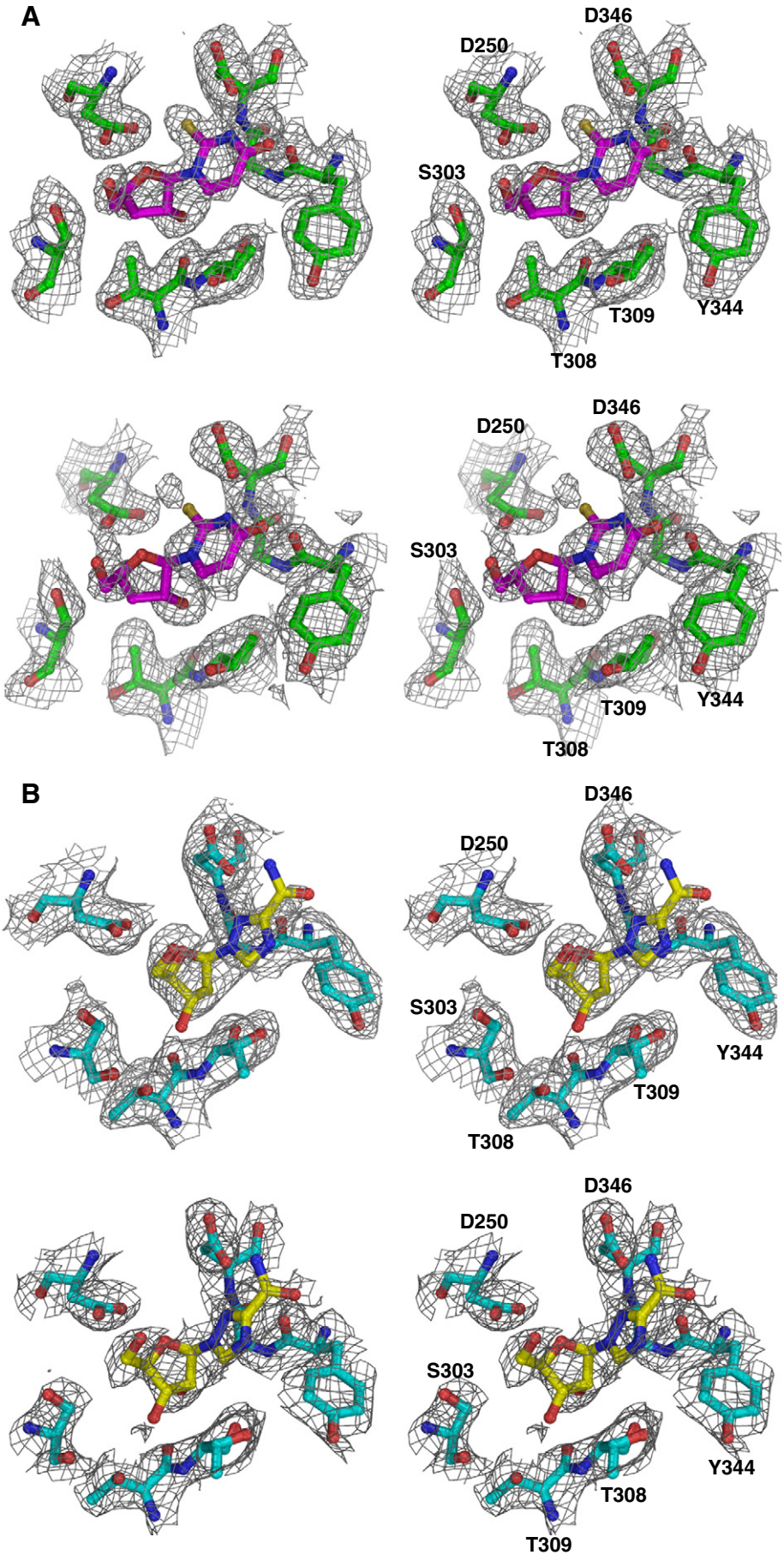
A
D346
D250
S303
T309
Y344
T308
D346
D250
S303
T309
Y344
T308
B
D346
D250
S303
Y344
T309
T308
D346
D250
S303
Y344
T308
T309

was very different from that of the 5FU, whereas that of Arg185 did not change significantly. In addition, residues including Asp250, Ser303, Thr308, Thr309, Asn312, Tyr344, and Gly345 were involved in the interaction with 2TU or ribavirin (see below), while the same interactions were not found in 5FU binding (Lee et al., 2011). Taken together, the binding of 2TU or ribavirin to the enzyme appears to result in more open active site structures, in comparison to that of native or 5FU complex structure.

Interaction of MNV-1 RdRp active site with 2TU or ribavirin

Binding mode of 2TU or ribavirin in MNV-1 RdRp is quite similar to that observed in other ligand-bound structures of RdRp. However, the position of ligands at the active site of the enzyme was found to be slightly shifted in comparison to the other RdRp structures (Ferrer-Orta et al., 2007; Zamyatkin et al., 2008, 2009), which may be attributed to the absence of RNA and triphosphate. The triphosphate moieties of ligands are known to interact with basic Arg residues in the active site. They are also known to have a significant effect on the electron density of ligands (Campagnola et al., 2011). In the absence of triphosphate moiety, the ligands (2TU and ribavirin) can be differently oriented in the active site of MNV-1 RdRp. A comparative analysis with the HuNoV structure (3H5Y) shows that the orientation of ribose ring is quite similar in both the cases (Supplementary Fig. S5). The ligands in our structures are non-phosphorylated and revealed different orientation from the already known one. The orientation reported in this manuscript was the best fit after many attempts with different orientations for these non-phosphorylated ligands. However, we do not rule out the possibility that the presence of phosphate at the ribose ring may orient the ligands similar to the already known conformations. In both the 2TU and ribavirin-bound complex structures, the 2′-hydroxyl group of the ribose ring accepts a hydrogen bond with the side chain of Asn312 and donates a hydrogen bond to Thr309 (Fig. 3B). On the contrary, in HuNoV CTP complex (PDB ID: 3H5Y), 2′-hydroxyl group accepts a hydrogen bond from Asn309 and donates a hydrogen bond to Ser300 (Zamyatkin et al., 2008). The highly conserved Ser303 residue (corresponding to Ser300 of HuNoV) in MNV-1 RdRp is far from the 2′-hydroxyl group to accept a hydrogen bond (5–7 Å) and instead makes hydrogen bonds with two water molecules in both the 2TU and ribavirin structures (Fig. 3B). Thr309 also forms H-bond with the 3′-hydroxyl group of ribose ring in the 2TU complex structure. These residues are well conserved at the active site of viral RdRp proteins. The amino acid residue Asp250 (corresponding to Asp247 of HuNoV) interacts directly with the 5′-hydroxyl group of 2TU as well as a water molecule.

Asp250, Ser303, Tyr344, Gly345 and Asp347 at the active site form both polar and hydrophobic interactions with 2TU and a number of water molecules are found to stabilize the interactions of the ligand with the active site residues. The uracil ring of 2TU is positioned in a pocket formed by residues Asp250, Tyr344, Asp346, and Asp347. Notably, the S atom at the uracil ring is interacting with the carboxyl groups of Asp250 and the N3 atom interact with Asp346 by forming hydrogen bonds. In contrast, Asp250 forms a hydrogen bond with the 4′-hydroxyl group of ribose ring through a water molecule in the ribavirin-bound structure (Fig. 3B). The ribose ring of ribavirin induces a slight shift in the backbone of Ser303 and Thr309 to accommodate the larger size of ribavirin, while that of 2TU is shifted towards Asp250 by 1.2 Å, compared with that of ribavirin. The ligand is further stabilized by the formation of a hydrogen bond between N2 and N3 of ribavirin and the carboxyl group of Asp346. Besides these, hydrophobic interactions between the ligand and amino acids Ser303, Thr309 and Gly345 have been observed in the ribavirin complexed structure. This highly conserved pattern of interactions is known to be responsible for distinguishing ribonucleotides from 2′-deoxyribonucleotide.

A schematic diagram of the interactions was generated using LIGPLOT (Fig. 3C) (Wallace et al., 1995). Notably, the two arginine residues Arg185 and Arg395 are not involved in direct interactions with 2TU. Only the 4-hydroxyl group of 2TU is forming a weak hydrogen bond to a water molecule which in turn interacts with Arg185. In contrast, the side chain of Arg395 adopts a different rotamer conformation in the ribavirin complex structure. The carboxamide group of ribavirin is hydrogen bonded to both Arg185 and Arg395 through a water molecule. Arg185 which is highly conserved is known to bind to the rNTP α-phosphate group, occupying a similar position in all available viral RdRp structures including distantly related HIV reverse transcriptase (Zamyatkin et al., 2008). Arg395 which is highly flexible together with Arg185 is implicated in coordination with phosphate groups of bound nucleotides. Our complex structures thus strongly suggest that Arg185 and Arg395 determine the orientation of ribavirin and 2TU, giving rise to diverse modes of interaction in the absence of phosphate and RNA, and the difference in interactions may be attributed to smaller size of 2TU in comparison to ribavirin.

Ligand-induced conformational changes at the active site

In order to further analyze the structural changes taking place at the active site in the absence of RNA and phosphate groups, we compared the structures of the MNV-1 RdRp complexes with HuNoV RdRp in complex with RNA and CTP (PDB IDs: 3BSO and 3H5Y) (Zamyatkin et al., 2008, 2009). The sequences of MNV-1 and HuNoV RdRps have a high similarity (59%) and the active site residues interacting with the ligands are identical in the two proteins, except for Thr309 in MNV-1 RdRp which corresponds to Ser306 in HuNoV RdRp. The overall r.m.s.d. difference of the superposition was found to be 1.0 Å. However, the ligands in MNV-1 RdRp complexes show a slightly different orientation from that of CTP, which is possibly due to the presence of triphosphate and RNA molecule which can make Watson and Crick hydrogen bonding with incoming rNTPs or their analogues. In our complex structures, surprisingly, the absence of RNA or triphosphate does not seem to affect the ligand binding of 2TU or ribavirin at the active site of MNV-1 RdRp, where the amino acid residues adopt a different rotamer conformation (Fig. 3B). Both Arg185 and Arg395 are known to be important for the ligand interaction in the presence of triphosphate group. The phosphate group of CTP in the HuNoV RdRp complex is oriented closer to (Arg182), thereby making a direct hydrogen bond (Supplementary Fig. S5). Importantly, the side chain conformation of Arg185 in MNV-1 RdRp is not affected even in the absence of RNA and phosphate. Arg395 is closer to the active site in comparison to its HuNoV counterpart (Arg392) which is too far away (~7 Å) to interact with CTP, but it adopts different conformations depending on the presence or absence of ligand, as evident from its high B-factor in the ligand bound structures. In order to understand further regarding the binding mode in different RNA polymerases, we compared our MNV-1 ligand structures with some poliovirus RdRp (PDB IDs: 2IM0 and 3OL7) reported earlier (Gong and Peersen, 2010; Thompson et al., 2007). The active site residues are highly conserved and GDD motifs of MNV-1 RdRp are well superposed with that of poliovirus RdRp. The active site residues which are involved in ligand interaction were well superposed with their corresponding partners in both structures. The ligand was inversely oriented in MNV-1 RdRp in comparison to poliovirus ligands. The ribose ring was found to be shifted by a distance of 3.5–5.0 Å in poliovirus RdRp. The difference in position as well as orientation can be attributed to triphosphate moiety in

Fig. 2. MNV-1 RdRp ligand complex and electron density maps. (A) Stereoviews of the $2|F_o|-|F_c|$ electron density maps (upper) and composite omit maps (lower panel) for 2TU in complex with MNV-1 RdRp are shown at 1.0σ and 0.8σ. The composite omit map is colored in grey. (B) Stereoviews of the $2|F_o|-|F_c|$ Fourier electron density maps (upper) and composite omit maps (lower) for ribavirin in complex with MNV-1 RdRp is shown at 1.0σ and 0.9σ. The composite omit map for ribavirin is colored in black.

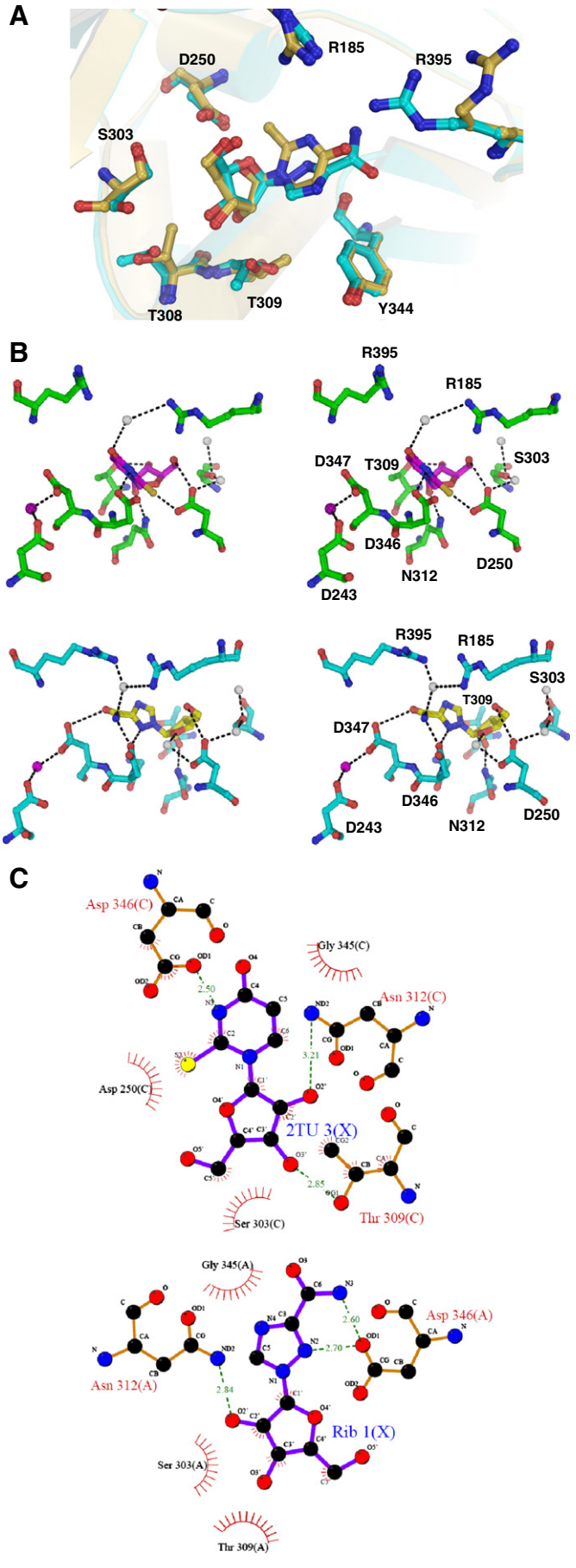

the ligands, which induces different conformational changes in the active site in comparison to the non-phosphorylated ligands.

Metal ion bound in MNV-1 RdRp complexes

In the native MNV-1 RdRp structure, the position of a metal ion which was confirmed in anomalous difference maps clearly showed a peak possibly for Mn^{2+} ion (Lee et al., 2011). Although the enzyme catalysis of RdRp was suggested to be mediated by two metal ion mechanism (Steitz, 1998), only one metal ion could be modeled in the vicinity of the active site. This metal ion was coordinated with the carboxylate groups of Asp243 and Asp347 and the main chain carbonyl atom of Ser392 in ranges from 2.6 to 2.8 Å (Fig. 3B). A water molecule modeled in close proximity of the metal ion was shown to interact with Asp243 and Asp347 in the 2TU or ribavirin complexes. The position of metal ion was found to be similar to that of HuNoV RdRp (3H5Y), where Asp347 (corresponding to Asp344 in HuNoV-1 RdRp) interacts with the metal ion. Asp346 in MNV-1 RdRp is superimposed well with its HuNoV counterpart (Asp343), which is shown to interact with the water molecule that is modeled instead of a metal ion in MNV-1 RdRp. Notably, the side chains of both Asp243 and Asp245 are oriented differently from their HuNoV counterparts (Asp242 and Asp243, respectively). A total of four metal ions were found at the active site of the CTP-bound structure of HuNoV RdRp (Zamyatkin et al., 2009). The absence of the second peak for Mn^{2+} ions in anomalous difference maps of MNV-1 RdRp might be due to the fact that this site may not always be occupied by Mn^{2+} ion, and instead either Mg^{2+} or a water molecule that is present at the active site. Interestingly, a significant difference in the position of the metal ion was observed in the 5FU-bound structure, which led to a different orientation of the side chains of Asp243 and Asp245 in the 5FU-bound structure of MNV-1 RdRp (Lee et al., 2011). The corresponding aspartate residues (Asp238 and Asp239) of FMDV RdRp are involved in metal binding where only one Mn^{+2} ion was reported at the active site (Ferrer-Orta et al., 2007). The network of interactions in the RdRp–ribavirin complex is also similar to that of the complex of FMDV RdRp with RTP.

Implications of ribavirin or 2TU binding to RdRp

Acute gastroenteritis caused by norovirus is a potential threat to human health, but effective antivirals or vaccines against this virus are not yet available. A number of RNA virus mutagens other than ribavirin are known (Holland et al., 1990; Lee et al., 1997), but they are unacceptable for use in humans at the necessary doses due to high cellular toxicity (Crotty et al., 2002). Ribavirin has been used as an antiviral prodrug which is metabolized to active 5′-monophosphate, diphosphate and triphosphate *in vivo* (Wu et al., 2003). In this study, the structures of MNV-1 RdRp-2TU and RdRp–ribavirin complexes confirm the binding of the ligand at the active site of viral polymerases, which is complemented by the DSF results.

Our biochemical studies revealed stronger inhibitory effect of 2TU on the replication of MNV-1 in RAW 264.7 cells, compared to that of ribavirin. The compound 2TU was also found to have an inhibitory effect on the viral growth in FCV and was the most effective inhibitor of viral polymerase activity among 5-iodouridine, pseudouridine, 5-methyluridine, 6-azauridine, and ribavirin (Belliot et al., 2005). The high potency of 2TU is now confirmed by our studies on MNV-1 in

Fig. 3. Active site in MNV-1 RdRp complex structures. (A) Superposition of the active sites of MNV-1 RdRp complexed with 2TU (yellow) and ribavirin (cyan). (B) Stereo-view of the 2TU (upper) and ribavirin (lower) at the active site of MNV-1 RdRp. 2TU and ribavirin are shown in a ball and stick model in magenta and yellow color, respectively. Purple sphere represents the metal ion, while white sphere represents water molecules. Dotted lines represent the various possible interactions. (C) The mode of interactions are represented by LIGPLOT in one of the chains of 2TU (upper) and ribavirin (lower) complexes.

RAW 264.7 cells as well as RdRp-2TU complex structure. However, the question remains: while the inhibitory effect of 2TU is much higher than that of ribavirin, their complex structures in this study did not show significant difference between two ligands. The number of interactions and the amino acid residues of RdRp involved in the interactions with 2TU are very similar to those with ribavirin if the ligand size is taken into consideration (Supplementary Table S1). It is also likely that 2TU may bind to other viral or host factors which may influence on viral replication. Nevertheless, low cellular toxicity and highly antiviral activity of 2TU on MNV-1 makes it an obvious choice for the search of novel antiviral pharmacophores. Further studies will be done for the search of novel lead compounds based on 2TU nucleus which can be effective in norovirus inhibition.

In conclusion, our structures reveal the binding modes of 2TU and ribavirin in norovirus, which highlights the conserved network of interactions involved in viral enzyme catalysis in the absence of RNA and phosphate groups in the ligand. As the structure of RdRp has been found to be conserved across different viruses, the structural results presented here will encourage the rational design of novel antiviral based on the 2TU and ribavirin nucleus as well as related pharmacophores. The absence of RNA and phosphate groups from our structure further opens up ample scope to use this as the starting model for designing some non-nucleoside based inhibitors which are still missing for calicivirus RdRp. Such studies will be helpful in our understanding of the viral enzyme catalysis and will make us better prepared against the RNA virus.

Materials and methods

Plasmid preparation and protein purification

Subcloning, protein extraction and purification of MNV-1 RdRp used for the structural studies have been done as described previously (Lee et al., 2011).

Effect of 2TU and ribavirin on MNV-1 infected RAW 264.7 cells

RAW 264.7 cells were grown in Dulbecco's Modified Eagle's Medium (DMEM) (Invitrogen, Grand Island, NY, USA) supplemented with 10% heat-inactivated fetal bovine serum (Sigma-Aldrich, St. Louis, MO, USA) and 1% penicillin and streptomycin (Invitrogen, Grand Island, NY, USA). MNV-1 was propagated in RAW 264.7 cells in DMEM Medium (without supplement) for 3–4 days and the titer was observed as 4×10^5 PFU/ml by plaque assay. Amplified MNV-1 viral stocks were stored at −70 °C.

The inhibitory effect of 2TU (Berry and Associates, USA) or ribavirin (Sigma-Aldrich, St. Louis, MO, USA) on MNV-1 was analyzed by cytopathic effects (CPE) inhibition assay, plaque reduction assay and RT-PCR. RAW 264.7 cells were seeded in 96-wells at a density of $1–2\times10^5$ cells/well 12–24 hrs prior to the experiments. When the confluence of RAW 264.7 cells reached 70–80% they were infected with MNV-1 (MOI 0.01). MNV-1 and an inhibitor were added into these cells in three different ways. First, MNV-1 was infected into confluent RAW 264.7 cells in the absence or presence of 2TU or ribavirin. Second, MNV-1 was pre-infected into confluent RAW 264.7 cells for 1 hr and 2TU or ribavirin was added in various concentrations (0–100 μM). Third, confluent RAW 264.7 cells were pre-treated with 2TU or ribavirin for 1 hr in different concentrations (0–100 μM), which was then infected with MNV-1 (MOI 0.01). The virus infected cells were incubated for 3 additional days at 37 °C under 5% CO_2 atmosphere and MNV-1 induced CPE was determined by MTT cell viability reduction assay. The absorbance was measured at 570 nm using a multiplate reader (Molecular devices, Spectro Max M2). MNV-1 induced CPE was assessed by monitoring the absorbance of non-infected cells minus that of virus infected non-treated cells (mock treated cells). Cell survival in the presence of 2TU or ribavirin was determined by comparing with mock treated cells. Values obtained from non-infected cells and cell infected by MNV-1 in the absence of 2TU or ribavirin were set to 100% and 0% (y-axis), respectively, and % of control was calculated as $(Ab-Absmnv\text{-}1)/(Absnoninfected\ cell-Abs)\times100$. All the experiments were replicated three times to minimize the error. Ribavirin and 2TU were used in non-cytotoxic range (0 to 100 μM). The antiviral activity was expressed as mean ± SD for three independent experiments. Means were evaluated by one-way ANOVA and used to compare the difference between the each group using Post-Hoc test by Ducan's method. P value of <0.05 was considered statistically significant.

Plaque reduction assay

Plaque reduction assay was carried out to compare the effect of ligands on the replication of MNV-1. RAW 264.7 cells were seeded into 24-well plates with DMEM, 5% FBS and 1% penicillin-streptomycin at a density of 1.5×10^6/well. After 12–16 hrs RAW 264.7 cells with MOI 0.1–0.001 were infected with MNV-1. A ligand (2TU or ribavirin) at a concentration range of 10–100 μM was added simultaneously or post virus infection. Cells were grown for 42 hrs at 37 °C under 5% CO_2, and were fixed and stained with 4% formaldehyde 0.5% crystal violet.

RT-PCR analysis

RAW 264.7 cells were seeded into 6-well plates with DMEM, 5% FBS and 1% penicillin–streptomycin at a density of $4–5\times10^6$/well. After 12–16 hrs, 10 μM 2TU or 100 μM ribavirin was simultaneously treated during MNV-1 inoculation (MOI 0.01) onto RAW 264.7 cells for 1 hr and ligands were removed from cells. Cells were incubated with fresh complete media for 1 or 2 days. In case of post-treatment, 10–100 μM 2TU or 100 μM ribavirin was treated into complete media after MNV-1 infection onto RAW 264.7 cells for 1 hr. At

Table 1
Data and refinement statistics.

	Ribavirin	2TU
Data statistics		
Wavelength (Å)	1.000	1.000
No. of reflections (unique)	564,425 (78,946)	630,236 (113,874)
Resolution range (Å)	50.0–2.50 (2.59–2.50)	50.0–2.20 (2.28–2.20)
Completeness (%)	100 (100)	99.4 (98.6)
R_{merge} (%)*	9.30 (46.1)	11.1 (46.1)
I/sigma	21.41 (4.65)	12.5 (2.33)
Mean redundancy	7.1	5.5
Space group	C2	C2
Unit cell parameters	$a=119.9$	$a=120.7$
	$b=196.0$	$b=195.9$
	$c=109.2$	$c=109.3$
	$\alpha=\gamma=90°\beta=114°$	$\alpha=\gamma=90°\beta=114°$
Refinement statistics		
Resolution range (Å)	47.84–2.50	31.62–2.20
No. of reflections	78,903	113,865
R/R_{free} (%)	18.1/22.8	20.2/25.2
r.m.s Deviation		
Bonds (Å)	0.008	0.009
Angles (°)	1.14	1.22
Number of water molecules	483	543
Average B (Å^2)	29.51	27.9
Ramachandran statistics		
Most favored region (%)	91.4	89.3
Additionally allowed region (%)	7.5	8.4
Outliers (%)	0.5	0.9

*$R_{merge}=\Sigma|I-\langle I\rangle|/\Sigma\langle I\rangle$, where I and $\langle I\rangle$ are the measured and averaged intensities of multiple measurements of the same reflection, respectively. The summation is over all the observed reflections.

**$R=\Sigma|F_o-F_c|/\Sigma|F_o|$ calculated for all observed data. $R_{free}=\Sigma|F_o-F_c|/\Sigma|F_o|$ calculated for a specified number of randomly chosen reflections that were excluded from the refinement.

the post-infection for 24–48 hrs, cells were harvested and viral RNA was extracted by RNeasy kit (QIAGEN, Valencia, CA, USA), according to the manufacturer's instructions. OligodT, random hexamer and RdRp primers (Bioneer, Daejon, Korea) were used to synthesize cDNA by MMLV reverse transcriptase (RT-&GO™ Master Mix kit, MP, USA) and were analyzed by RT-PCR. GAPDH (GAPDH-F, AACGACCCCTTCATTGAC and GAPDH-R, TCCACGACATACTCAGCAC) was used as endogenous control gene. PCR was performed using the RdRp and GAPDH primers with an initial denaturing at 94 °C for 5 min, followed by 35 cycles of denaturing at 94 °C for 1 min, annealing at 60 °C for 1 min, and extension at 72 °C for 1 min and then a final extension at 72 °C for 5 min. PCR products were subjected to 1.5% agarose gel electrophoresis.

Isothermal titration calorimetry (ITC)

ITC experiments were performed using VP-ITC calorimeter from Microcal (Northampton, MA, USA). Experiments were carried out by titrating MNV-1 RdRp (50 μM) with 2TU (1.5 mM) at 15 °C. A total of 30 injections were performed at a spacing of 300 s and a reference power of 10 μcal/sec. Control experiments to determine the heat of dilution for each injection were performed by injecting the same volume of 2TU into sample cell containing only buffer. The heat of dilution generated by the compounds was subtracted and the binding isotherms were plotted and fit to a single site binding model using origin ITC software.

Differential scanning fluorimetry (DSF)

In order to confirm the binding of 2TU or ribavirin to MNV-1 RdRp we used the DSF method which measures the shift in T_m upon ligand binding. MNV-1 RdRp at a concentration of 1 mg/ml (16.5 μM) was incubated with a ligand (2TU or ribavirin) in concentrations ranging from 1 to 20 mM overnight. Samples were prepared by mixing 0.5 μl (500-fold) SYPRO Orange in the protein mixture and incubated at 25 °C for 30 s. It was then followed by temperature increment at the rate of 0.5 °C every 30 s for 50 min and relative fluorescence units were recorded using Mx3005P differential scanning fluorimetry (Stratagene, CA, USA). The excitation wavelength was 492 nm and the emission wavelength was 610 nm. T_m was calculated from the maxima of the first derivative of relative fluorescence units/temperature using MxPro QPCR Software.

Crystallization and data collection

The homogenous fractions of the purified RdRp were pooled and concentrated up to ~3 mg/ml using a 10 kDa cut-off membrane filter. The concentrated RdRp was incubated separately with 20 mM 2TU or ribavirin at 4 °C overnight and crystals were screened by sitting drop method using commercial kits (Emerald Biosystems, Bainbridge Island, USA). Good quality crystals for ribavirin were observed in 2–3 days after incubation at room temperature in 1.26 M ammonium sulphate, CHES (pH 9.5) and 0.2 M NaCl, which was further refined by hanging drop method with varying pH range (9.0–10.0) and ammonium sulphate concentration (0.8-1.4 M). For 2TU diffraction quality crystals were found in 2.0 M ammonium sulphate, cacodylate pH 6.5 and 0.2 M sodium chloride.

Diffraction quality crystals were transferred to the mother liquor (approximately 30% higher concentrations than the reservoir solution) containing 22% glycerol as cryoprotectant prior to mounting for data collection. Crystals diffracted at a resolution of 2.5 Å for ribavirin while the resolution for 2TU was 2.2 Å. In order to identify the position of a metal ion, a crystal was soaked in 10 mM $MnCl_2$ for 30 minutes and anomalous data were collected at the wavelength of 1.89 Å. Diffraction data were collected with crystals flash-cooled at 100 K in a stream of liquid N_2 using a synchrotron radiation source, Beamline 4A at Pohang Light Source (Quantum CCD detector, ADSC, USA). The data were processed using HKL 2000 (Otwinowski and Minor, 1997). The crystals were of space group C2 with unit cell dimensions $a=120$, $b=196$, $c=109$, $\alpha=\gamma=90$, $\beta=114$ with three monomers in the asymmetric unit.

Structure solution and refinement

The ligand complex structure was solved using CCP4 for molecular replacement (Vagin and Teplyakov, 1997), employing a previously solved structure of the same protein complexed with 5-fluorouracil (5FU) (PDB ID: 3NAI) as a search model. Molecular replacement gave a single prominent solution after rotation and translation function. The initial solution was optimized by rigid body refinement, which produced a clearly interpretable electron density for the overall structure. Density for 2TU or ribavirin was clearly observed at the active site of MNV-1 RdRp. Manual adjustment of the backbone and side chain was done in Coot (Emsley and Cowtan, 2004). The side chains were assigned easily to the model using the electron density map which was helpful in avoiding any model bias during molecular replacement. Crystallographic refinement was carried out using the programs PHENIX and Refmac5 (Adams et al., 2010; Murshudov et al., 1997). Difference Fourier maps with coefficients $2|F_o|-|F_c|$ and $|F_o|-|F_c|$ were used to model 2TU and ribavirin interacting with amino acid residues at the active site. After a few rounds of model building water molecules were then added using the F_o-F_c map peaks above 3.0σ, if the B factors were below 60 $Å^2$ after refinement. The value of R_{free} has been used as an indicator to validate the water picking and refinement procedure and to avoid any possible over fitting of the data. At the end of refinement residues 1–4 and 493–509 could not be modeled in both ribavirin and 2TU complexed data due to poor electron density in these regions. The C-terminal His tag was also missing in all the three chains. The R/R_{free} values were 18.1/22.8%, and 20.2/25.2% for ribavirin and 2TU complex data respectively. Data quality and refinement statistics are presented in Table 1.

Supplementary materials related to this article can be found online at doi:10.1016/j.virol.2012.01.016.

Acknowledgments

We thank the staffs at beamlines 4A Pohang Light Source for help with data collection. This work was supported by a grant of the Korea Healthcare Technology R&D Project, Ministry of Health, Welfare and Family Affairs, Korea (A085119 and A080742).

Coordinate accession numbers: The atomic coordinates and structure factors have been deposited in the Protein Data Bank (www.rcsb.org) with PDB IDs: 3SFG for 2TU and 3SFU for the ribavirin complexed data.

References

Adams, P.D., Afonine, P.V., Bunkoczi, G., Chen, V.B., Davis, I.W., Echols, N., Headd, J.J., Hung, L.W., Kapral, G.J., Grosse-Kunstleve, R.W., McCoy, A.J., Moriarty, N.W., Oeffner, R., Read, R.J., Richardson, D.C., Richardson, J.S., Terwilliger, T.C., Zwart, P.H., 2010. PHENIX: a comprehensive Python-based system for macromolecular structure solution. Acta Crystallogr. D Biol. Crystallogr. 66, 213–221.

Belliot, G., Sosnovtsev, S.V., Chang, K.O., Babu, V., Uche, U., Arnold, J.J., Cameron, C.E., Green, K.Y., 2005. Norovirus proteinase-polymerase and polymerase are both active forms of RNA-dependent RNA polymerase. J. Virol. 79, 2393–2403.

Campagnola, G., Gong, P., Peersen, O.B., 2011. High-throughput screening identification of poliovirus RNA-dependent RNA polymerase inhibitors. Antiviral Res. 91, 241–251.

Chang, K.O., George, D.W., 2007. Interferons and ribavirin effectively inhibit Norwalk virus replication in replicon-bearing cells. J. Virol. 81, 12111–12118.

Crotty, S., Maag, D., Arnold, J.J., Zhong, W., Lau, J.Y., Hong, Z., Andino, R., Cameron, C.E., 2000. The broad-spectrum antiviral ribonucleoside ribavirin is an RNA virus mutagen. Nat. Med. 6, 1375–1379.

Crotty, S., Cameron, C., Andino, R., 2002. Ribavirin's antiviral mechanism of action: lethal mutagenesis? J. Mol. Med. 80, 86–95.

Emsley, P., Cowtan, K., 2004. Coot: model-building tools for molecular graphics. Acta Crystallogr. D Biol. Crystallogr. 60, 2126–2132.
Ferrer-Orta, C., Arias, A., Perez-Luque, R., Escarmis, C., Domingo, E., Verdaguer, N., 2007. Sequential structures provide insights into the fidelity of RNA replication. Proc. Natl. Acad. Sci. U. S. A. 104, 9463–9468.
Gong, P., Peersen, O.B., 2010. Structural basis for active site closure by the poliovirus RNA-dependent RNA polymerase. Proc. Natl. Acad. Sci. U. S. A. 107, 22505–22510.
Green, K.Y., 2007. Caliciviruses: The Noroviruses, In: Knipe, D.M., Howley, P.M. (Eds.), Fields virology, 5th ed. Wolters Kluwer Health / Lippincott Williams & Wilkins, Philadelphia ; London, pp. 949–979.
Hirata, A., Klein, B.J., Murakami, K.S., 2008. The X-ray crystal structure of RNA polymerase from Archaea. Nature 451, 851–854.
Hogbom, M., Jager, K., Robel, I., Unge, T., Rohayem, J., 2009. The active form of the norovirus RNA-dependent RNA polymerase is a homodimer with cooperative activity. J. Gen. Virol. 90, 281–291.
Holland, J.J., Domingo, E., de la Torre, J.C., Steinhauer, D.A., 1990. Mutation frequencies at defined single codon sites in vesicular stomatitis virus and poliovirus can be increased only slightly by chemical mutagenesis. J. Virol. 64, 3960–3962.
Karst, S.M., Wobus, C.E., Lay, M., Davidson, J., Virgin, H.W.t., 2003. STAT1-dependent innate immunity to a Norwalk-like virus. Science 299, 1575–1578.
Krissinel, E., Henrick, K., 2004. Secondary-structure matching (SSM), a new tool for fast protein structure alignment in three dimensions. Acta Crystallogr. D Biol. Crystallogr. 60, 2256–2268.
Lau, J.Y., Tam, R.C., Liang, T.J., Hong, Z., 2002. Mechanism of action of ribavirin in the combination treatment of chronic HCV infection. Hepatology 35, 1002–1009.
Lee, C.H., Gilbertson, D.L., Novella, I.S., Huerta, R., Domingo, E., Holland, J.J., 1997. Negative effects of chemical mutagenesis on the adaptive behavior of vesicular stomatitis virus. J. Virol. 71, 3636–3640.
Lee, J.H., Alam, I., Han, K.R., Cho, S., Shin, S., Kang, S., Yang, J.M., Kim, K.H., 2011. Crystal structures of murine norovirus-1 RNA-dependent RNA polymerase. J. Gen. Virol. 92, 1607–1616.
Lindesmith, L., Moe, C., Marionneau, S., Ruvoen, N., Jiang, X., Lindblad, L., Stewart, P., LePendu, J., Baric, R., 2003. Human susceptibility and resistance to Norwalk virus infection. Nat. Med. 9, 548–553.
Murshudov, G.N., Vagin, A.A., Dodson, E.J., 1997. Refinement of macromolecular structures by the maximum-likelihood method. Acta Crystallogr. D Biol. Crystallogr. 53, 240–255.
Ng, K.K., Pendas-Franco, N., Rojo, J., Boga, J.A., Machin, A., Alonso, J.M., Parra, F., 2004. Crystal structure of norwalk virus polymerase reveals the carboxyl terminus in the active site cleft. J. Biol. Chem. 279, 16638–16645.
Otwinowski, Z., Minor, W., 1997. Processing of X-ray diffraction data collected in oscillation mode. Methods Enzymol 276, 307–326.
Steitz, T.A., 1998. A mechanism for all polymerases. Nature 391, 231–232.
Thompson, A.A., Albertini, R.A., Peersen, O.B., 2007. Stabilization of poliovirus polymerase by NTP binding and fingers-thumb interactions. J. Mol. Biol. 366, 1459–1474.
Vagin, A., Teplyakov, A., 1997. MOLREP: an automated program for molecular replacement. J. Appl. Crystallogr. 30, 1022–1025.
Vedadi, M., Niesen, F.H., Allali-Hassani, A., Fedorov, O.Y., Finerty Jr., P.J., Wasney, G.A., Yeung, R., Arrowsmith, C., Ball, L.J., Berglund, H., Hui, R., Marsden, B.D., Nordlund, P., Sundstrom, M., Weigelt, J., Edwards, A.M., 2006. Chemical screening methods to identify ligands that promote protein stability, protein crystallization, and structure determination. Proc. Natl. Acad. Sci. U. S. A. 103, 15835–15840.
Wallace, A.C., Laskowski, R.A., Thornton, J.M., 1995. LIGPLOT: a program to generate schematic diagrams of protein–ligand interactions. Protein Eng. 8, 127–134.
Wobus, C.E., Karst, S.M., Thackray, L.B., Chang, K.O., Sosnovtsev, S.V., Belliot, G., Krug, A., Mackenzie, J.M., Green, K.Y., Virgin, H.W., 2004. Replication of Norovirus in cell culture reveals a tropism for dendritic cells and macrophages. PLoS Biol. 2, e432.
Wobus, C.E., Thackray, L.B., Virgin, H.W.t., 2006. Murine norovirus: a model system to study norovirus biology and pathogenesis. J. Virol. 80, 5104–5112.
Wu, J.Z., Lin, C.C., Hong, Z., 2003. Ribavirin, viramidine and adenosine-deaminase-catalysed drug activation: implication for nucleoside prodrug design. J. Antimicrob. Chemother. 52, 543–546.
Zamyatkin, D.F., Parra, F., Alonso, J.M., Harki, D.A., Peterson, B.R., Grochulski, P., Ng, K.K., 2008. Structural insights into mechanisms of catalysis and inhibition in Norwalk virus polymerase. J. Biol. Chem. 283, 7705–7712.
Zamyatkin, D.F., Parra, F., Machin, A., Grochulski, P., Ng, K.K., 2009. Binding of 2′-amino-2′-deoxycytidine-5′-triphosphate to norovirus polymerase induces rearrangement of the active site. J. Mol. Biol. 390, 10–16.